

Effect of KOH Concentration on the Microstructure and Electrochemical Properties of MAO-Coated Mg Alloy AZ31B

A. Fattah-alhosseini and M. Sabaghi Joni

(Submitted March 26, 2015; in revised form July 22, 2015; published online August 6, 2015)

In this study, the effect of KOH concentration on the electrochemical properties of micro-arc oxidation (MAO) coated Mg alloy AZ31B has been investigated. Also, the surface morphology and chemical composition of the MAO coatings have been characterized by scanning electron microscopy and x-ray diffraction. In MAO process, an increase in the concentration of KOH as a result of increase in the electrolyte electrical conductivity leads to a reduction in sparking which in turn improves the quality and the behavior of anodic coatings in the concentration of 2.5 M. Moreover, it can be concluded that the MAO coating shows its best protective behavior when KOH concentration is equal 2.5 M, and if the concentration is higher or lower than this value, the protective properties of MAO coating will decrease.

Keywords AZ31B, corrosion, MAO coatings, semiconducting properties

1. Introduction

The main drawback of Mg and its alloys is high corrosion rate, which is much higher when compared to many other competing materials, like steels or Al alloys. This behavior limits the range of applications of Mg and its alloys in industrial applications such as aerospace and automotive components. According to the Pourbaix diagram, Mg and its alloys corrode over a wide range of pH and potential (Ref 1). But at high pH (values over 11), in the passive region, the surface film is protective (Ref 2). This surface film forms an efficient barrier against the metal dissolution and undergoes a passivity breakdown under certain conditions, conversion of the barrier film within atmospheric corrosion or destruction of the protective surface film by several anions, such as chloride, bromide, nitrate, perchlorate, and sulfate (Ref 3).

A wide range of techniques, such as chemical conversion coating (Ref 4-8), physical vapor deposition (Ref 9, 10), spraying (Ref 11-13), plating (Ref 14-16), and laser surface modification (Ref 17, 18), have been employed to improve the corrosion resistance of Mg and its alloys. But recent studies have focused on the MAO process (Ref 19-42). MAO is a surface treatment which is done to create an oxide coating by anodic discharge deposition in a suitable electrolyte in high anodic voltage. This process can create a protective oxide-hydroxide layer which improves the surface properties of Mg and its alloys (Ref 43-46).

In MAO process, alkaline solutions are widely used as the primary electrolyte because of the high passivation susceptibility on Mg and its alloys and preventing the process of anodic dissolution (Ref 47). In addition, in order to improve the quality of the resulting coatings, increase the electrical conductivity of base electrolyte, and contribute certain elements within the MAO coatings, various additives are added to the base electrolyte (Ref 48-53). It is known that phosphate can produce a sustainable $Mg_3(PO_4)_2$ product to protect the Mg alloys (Ref 54-56). Borate is another additive under investigation. The reason for this choice is the rapid decomposition of $B_4O_7^{2-}$ that provides oxygen for the metal cations in the electric field, and contributes to the growth of the oxide layer on Mg alloys in the process of MAO like phosphate (Ref 57-59).

Although the extensive number of papers has been published in the field of corrosion behavior of the coatings formed on the Mg and its alloys during MAO process (Ref 19-59), little research has been focused on the semiconducting behavior of MAO coatings and their passivity properties in alkaline solutions. Hence, the primary objective of this study was investigation of role of electrolyte chemistry on the semiconducting properties of the MAO films formed on AZ31B Mg alloy. This is important because the key parameters in determining the transport of point defects and the kinetics of film growth are density and diffusivity of the defects in film, which can be determined by using the Mott-Schottky analysis methods. In this context, this research addresses the effect of the electrolyte concentration change parameter in determining the discharge characteristics, MAO coating quality, passive properties, and semiconducting behavior of MAO coatings compared to the AZ31B Mg alloy. In the formation of MAO coatings, electrolytes containing KOH with different concentrations were used as base electrolyte, and sodium phosphate and sodium borate with constant concentration were used as additives. Characteristics of resultant coatings were studied by SEM and XRD analysis. Potentiodynamic polarization and electrochemical impedance spectroscopy (EIS) measurements were applied in determining the passive properties and Mott-Schottky analysis in studies of semiconducting behavior.

A. Fattah-alhosseini and M. Sabaghi Joni, Department of Materials Engineering, Bu-Ali Sina University, 65178-38695 Hamedan, Iran. Contact e-mails: arash.fattah@gmail.com and a.fattah@basu.ac.ir.

2. Experimental Procedures

2.1 Preparation of MAO Coatings

AZ31B Mg alloy used in the present work has the following composition (in wt.%): Al, 2.6; Zn, 0.98; Mn, 0.43; Sn, 0.002; the balance being Mg (determined by emission spectroscopy analysis with a WAS Foundry Master Spectrometer). Samples cut into a size of 30 mm × 10 mm of a 1-mm-thickness plate were used as substrate in MAO process. All samples were ground to P2000 grit SiC water proof abrasive papers followed by cleaning with deionized water prior to coating. MAO of samples was done under unipolar mode, for 600 s using a constant current density (300 mA/cm²). In MAO process, sample was used as anode, while a stainless steel container was used as cathode. The electrolytes were alkaline solutions with different concentrations of KOH and containing Na₃PO₄·12H₂O and Na₂B₄O₇ as listed in Table 1. The selected concentration of Na₃PO₄·12H₂O and Na₂B₄O₇ is based on the previous investigations according to (Ref 56, 58, 60-63). After MAO processing the samples were washed with deionized water and dried.

2.2 Characterization of MAO Coatings

The surface morphology of prepared MAO coatings was examined under a JEOL JSM-840A scanning electron microscope. Also, the phase evaluation of samples was carried out by XRD analysis with Italstructures APD2000 diffractometer using CuKα radiation. The diffractometer was operated at a voltage and electrical current of 40 kV and 30 mA, respectively.

2.3 Electrochemical Measurements

All the electrochemical measurements were done in a conventional three-electrode flat cell under aerated conditions by using the μAutolab Type III/FRA2 system controlled by a personal computer. The counter electrode was a Pt plate, while the reference electrode was Ag/AgCl saturated in KCl. The 0.01 M NaOH solution was used as the test solution at 25 ± 1 °C. A set of three different specimens was tested at each electrochemical test, and all the reported electrochemical data are representative of the best values of three different samples. Prior to the electrochemical measurements, working electrodes were immersed at open circuit potential conditions for 1200 s in 0.01 M NaOH solution to form a steady-state condition. The electrochemical measurements were done in the following sequence:

Table 1 Electrolyte composition for the MAO-treated samples of AZ31B Mg alloy

	Electrolyte composition
Sample A	1.0 M KOH + 0.25 M Na ₃ PO ₄ ·12H ₂ O + 0.05 M Na ₂ B ₄ O ₇ ·10H ₂ O
Sample B	1.5 M KOH + 0.25 M Na ₃ PO ₄ ·12H ₂ O + 0.05 M Na ₂ B ₄ O ₇ ·10H ₂ O
Sample C	2.0 M KOH + 0.25 M Na ₃ PO ₄ ·12H ₂ O + 0.05 M Na ₂ B ₄ O ₇ ·10H ₂ O
Sample D	2.5 M KOH + 0.25 M Na ₃ PO ₄ ·12H ₂ O + 0.05 M Na ₂ B ₄ O ₇ ·10H ₂ O
Sample E	3.0 M KOH + 0.25 M Na ₃ PO ₄ ·12H ₂ O + 0.05 M Na ₂ B ₄ O ₇ ·10H ₂ O

- EIS tests were carried out at open circuit potential conditions and AC potential with the amplitude of 10 mV and normally a frequency range of 100 kHz to 100 mHz. For the EIS data modeling and curve-fitting method, the NOVA impedance software was used.
- Potentiodynamic polarization curves were measured potentiodynamically at a scan rate of 1 mV/s starting from -0.25 V (vs. E_{corr}) to 2.5 V_{Ag/AgCl}.
- Mott-Schottky analysis was carried out on the passive films of another set of MAO samples at a frequency of 1 kHz using a 10 mV AC signal and a step potential of 25 mV, in the cathodic direction.

3. Results and Discussion

3.1 Voltage-Time Characteristics of MAO Process

Since MAO coatings were created using a constant current density, a measure of voltage changes in terms of treatment time states the various stages of coating formation. Considering the voltage curves versus time, three different stages are recognized (Fig. 1):

In the first stage, the cell voltage shows a rapid and linear increase with time. The electric field provides the electromotive force for the transport of cations and anions in the electrolyte throughout the barrier layer and contributes to the thickness increase. The formation of a barrier layer is accompanied by the emission of oxygen bubbles. This stage is representative of common anodizing process trend (Ref 64). Increasing the thickness of the barrier layer, it acts as a resistor against the current flow. After this, the dielectric breakdown of the barrier layer occurs in areas where there is less resistance, resulting in the formation of small spark discharges in breakdown voltage (the second stage onset). Subsequently, the cell potential increases continuously. At this stage, the current flow only focuses on breakdown areas, leading to localized thickening of the oxide layer. New coating material formation causes resistance recovery against the current flow, while other areas with lower resistance are prone to breakdown. Therefore, a large number of fine white sparks can be seen moving randomly. Continuous oxide layer formation and breakdown

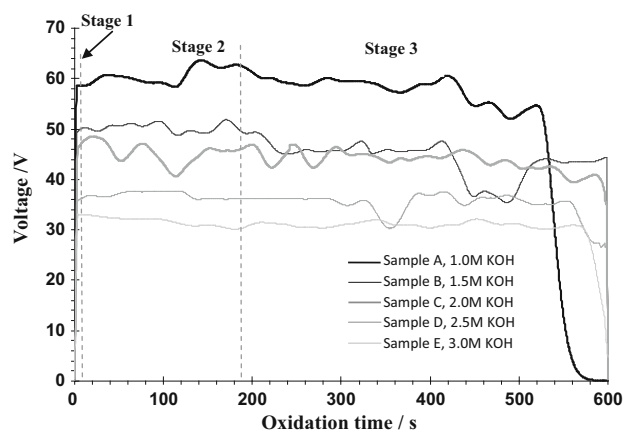


Fig. 1 Time vs. voltage curves of MAO-treated AZ31B Mg alloy samples (applied current density = 300 mA/cm²)

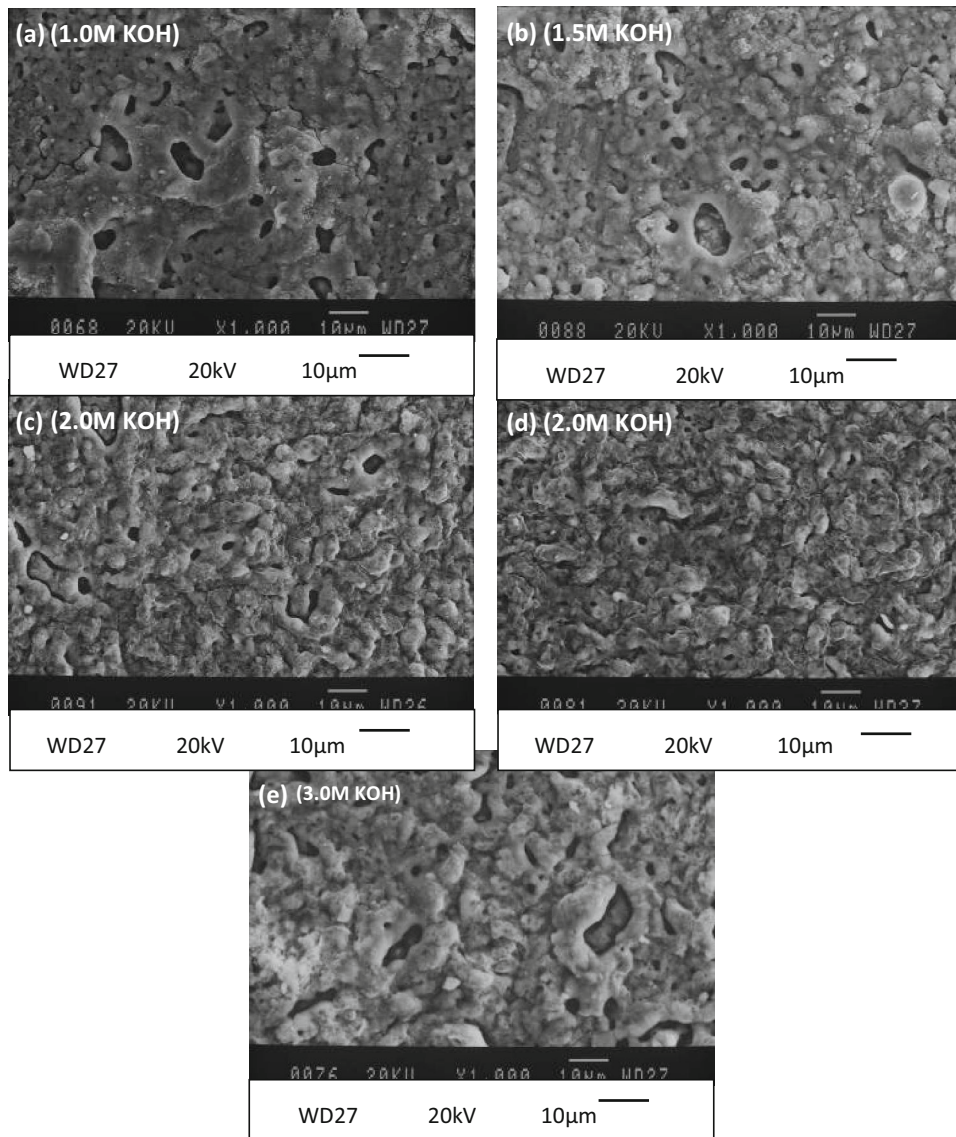


Fig. 2 SEM micro-graphs of AZ31B Mg alloy with MAO coatings: (a) Sample A, (b) Sample B, (c) Sample C, (d) Sample D, and (e) Sample E

cause the cell potential alteration. With time increase (the third stage), spark discharges grow in size with a change in color from white to orange. The sparks are discrete and move slowly across the surface and gradually disappear on the sample surface. Accordingly, the voltage decreases indicating the thickening of the oxide film and the end of coating process. It can be seen that the voltage response versus time in different solutions has demonstrated similar behavior. The effect of KOH concentration on ignition/breakdown voltage is obvious. An increase in the concentration of KOH has reduced ignition/breakdown voltage as a result of increased electrolyte conductivity which is in agreement with the results obtained by Cheng et al. (Ref 65) and Ko et al. (Ref 66).

3.2 SEM Characteristics

Figure 2 shows the scanning electron micro-graphs of MAO coatings. The morphological characteristics of coatings show the oxide grains with different diameters which are melted and

Table 2 Average pore size and porosity of MAO coatings

	Pore size (μm)	Porosity (%)
Sample A	4.67 ± 0.15	8.2
Sample B	3.97 ± 0.17	6.3
Sample C	3.56 ± 0.11	5.2
Sample D	3.45 ± 0.09	3.9
Sample E	5.90 ± 0.34	6.0

The \pm values refer to standard error of the mean

randomly distributed over the surface. The lumpy melting and sintering effect caused a rough surface formation. The presence of pores and micro-cracks, characteristic of MAO coatings, is quite evident. Pores are formed when the oxide is molten and gas bubbles are thrown out of micro-arc discharge channels (Ref 67, 68). Quick solidification of the molten oxide by the relatively cold electrolyte creates thermal stress in the oxide

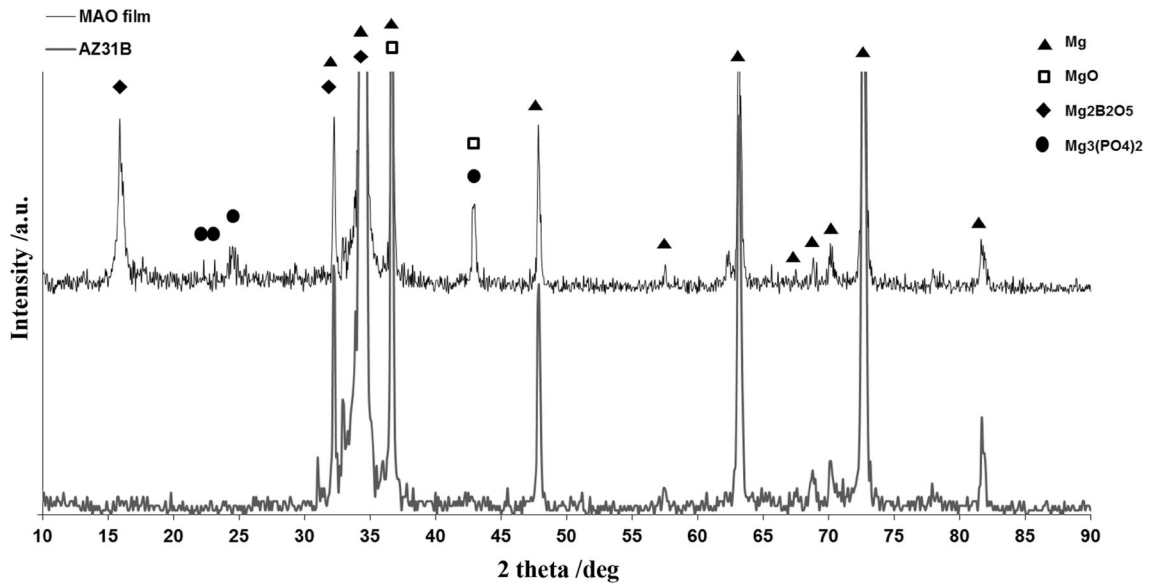


Fig. 3 XRD pattern of AZ31B Mg alloy with and without MAO coatings

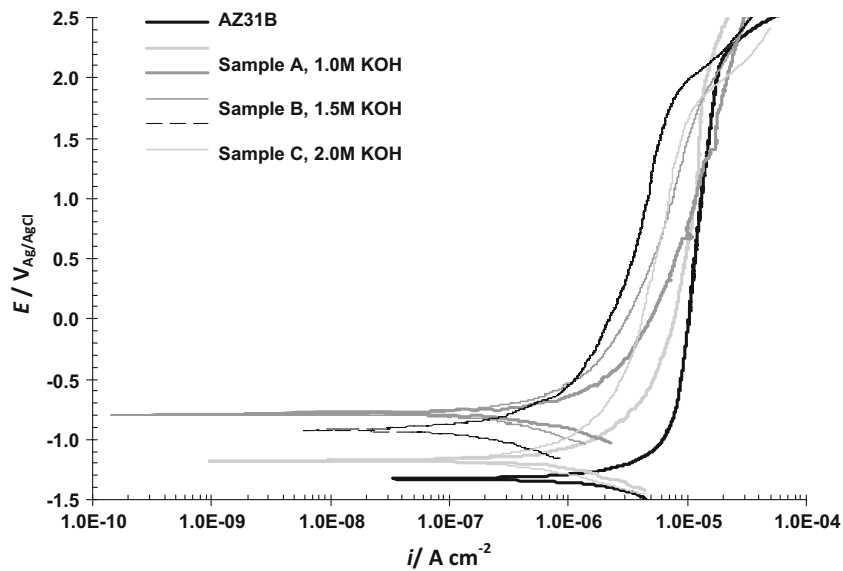


Fig. 4 Potentiodynamic polarization curves of AZ31B Mg alloy with and without MAO coatings in 0.01 M NaOH solution

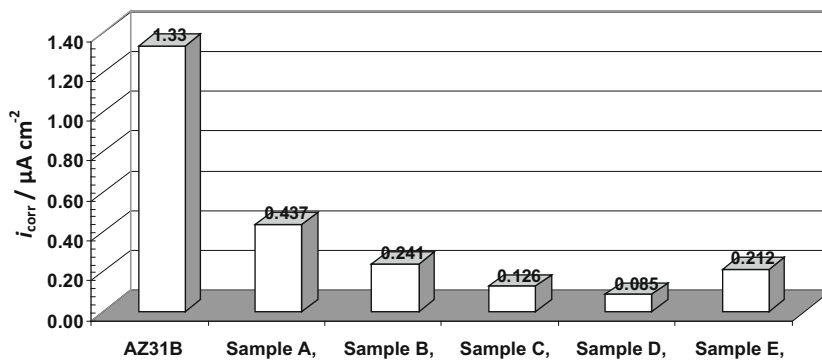


Fig. 5 Variations of the corrosion current density of AZ31B Mg alloy with and without MAO coatings in 0.01 M NaOH solution

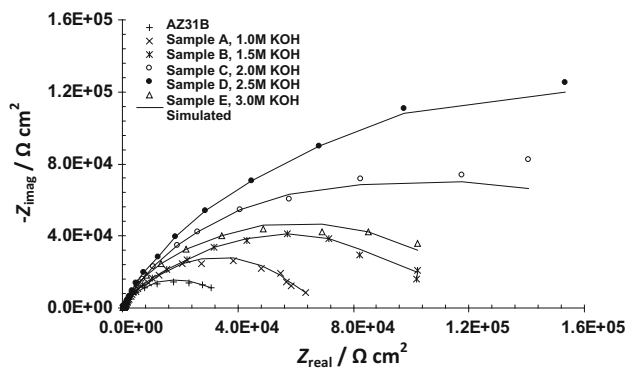


Fig. 6 Nyquist and Bode plots of AZ31B Mg alloy with and without MAO coatings in 0.01 M NaOH solution

layer, and when the stress is released, the micro-cracks are formed (Ref 68-71). As can be inferred from Fig. 2 and Table 2, morphology, average pore size, and porosity percentage are largely a function of spark potential which is in turn a function of the concentration and the electrical conductivity of the solution in the MAO process. With increasing KOH concentration of 1.0 to 2.5 M, as a result of increase in the electrical conductivity of the solution and ease of sparking, the pores' shapes in the center of the crater move from irregular and elliptical shape to a circle with a reduction in size. And the average pore size and porosity percentage decrease (Table 2). Generally, the presence of bigger pores or higher pore density on the surface of MAO coatings would facilitate quicker infiltration of the corrosive medium into the inner layer of the MAO coating and subsequently down to the substrate due to the increasing of the effective surface area and concentrating the corrosive medium into these microspores. In addition, the oxide grain size due to the ease of sparking decreases with increasing concentration of KOH, so that in 2.5 M KOH concentration, the coating is more homogeneous and oxide nodules are smaller. However, increasing the concentration of KOH to 3.0 M causes a deleterious effect on the obtained coating porosity. The reason for this can be a large increase in electrical conductivity spreading severe spark discharge leading to the formation of the MAO coating with large micro-pores (Ref 66).

3.3 Phase Analyses

The XRD patterns of AZ31B Mg alloy with and without MAO coating are depicted in Fig. 3. XRD spectrum after MAO treatment indicates that MgO and Mg₂B₂O₅ are the new phases in the MAO film compared to that of in the substrate. It also can be seen that anions from the Na₃PO₄·10H₂O and Na₂B₄O₇·5H₂O additives contributed to react with Mg²⁺ from substrate dissolution and formed the compounds in the coating such as Mg₃(PO₄) and Mg₂B₂O₅.

3.4 Potentiodynamic Polarization Measurements

Potentiodynamic polarization curves of AZ31B Mg alloy with and without MAO coatings in 0.01 M NaOH solution are shown in Fig. 4. It is observed the AZ31B Mg alloy with and without MAO coatings exhibits the same curve shapes, where the current changes smoothly and linearly around the rest potential manifesting cathodic and anodic Tafel behavior.

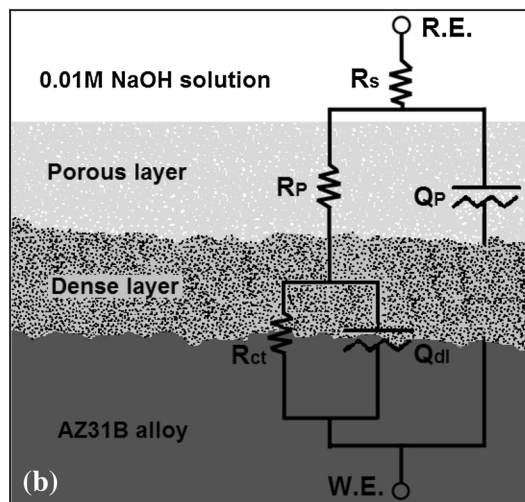
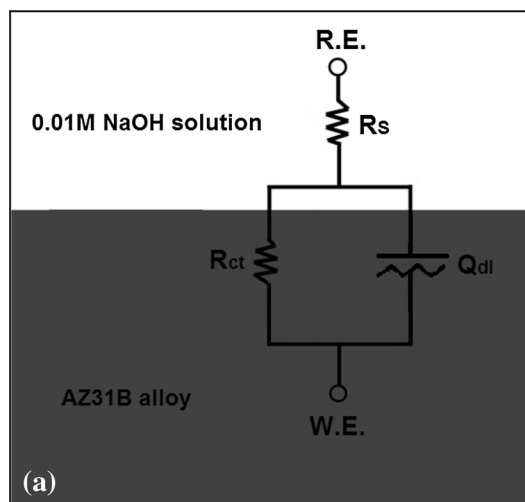


Fig. 7 Equivalent electrical circuits used to fit the impedance data of (a) AZ31B Mg alloy and (b) AZ31B Mg alloy with MAO coatings

The corrosion current density (i_{corr}) was calculated by Tafel extrapolation of the linear part of the cathodic branch back to the corrosion potential with an accuracy of more than 95% of the points more negative to E_{corr} by 50 mV (Ref 72, 73). The variation of the corrosion current density of AZ31B Mg alloy with and without MAO coatings in 0.01 M NaOH solution is illustrated in Fig. 5. A maximum corrosion current density is observed for the AZ31B Mg alloy, and a minimum value is recorded for the sample D. These results show that the MAO process can significantly improve the corrosion resistance of the AZ31B Mg alloy.

Also, it is observed that the corrosion current density of AZ31B Mg alloy with MAO coatings decreases with increasing the KOH concentration up to 2.5 M, while it increases when the KOH concentration reaches 3.0 M. This behavior is attributed directly to the pore size and porosity percentage. According to Table 2, with increasing KOH concentration of 1.0 to 2.5 M, the average pore size, and porosity percentage decrease. However, increasing the concentration from 2.5 M to 3.0 M causes a deleterious effect on the obtained coating porosity.

Table 3 Fitting results of EIS plots of AZ31B Mg alloy with and without MAO coatings based on the equivalent circuits in Fig. 7(a) and (b)

	R_p , $k\Omega\text{ cm}^2$	$CPE-C_p$, $\mu\text{F/cm}^2$	R_{ct} , $k\Omega\text{ cm}^2$	$CPE-C_{dl}$, $\mu\text{F/cm}^2$
AZ31B	39.8	13.6
Sample A	0.92	1.23	65.2	17.2
Sample B	0.54	1.61	102.8	21.4
Sample C	0.44	1.68	196.8	31.2
Sample D	0.35	1.82	385.1	32.1
Sample E	0.71	3.21	122.9	18.3

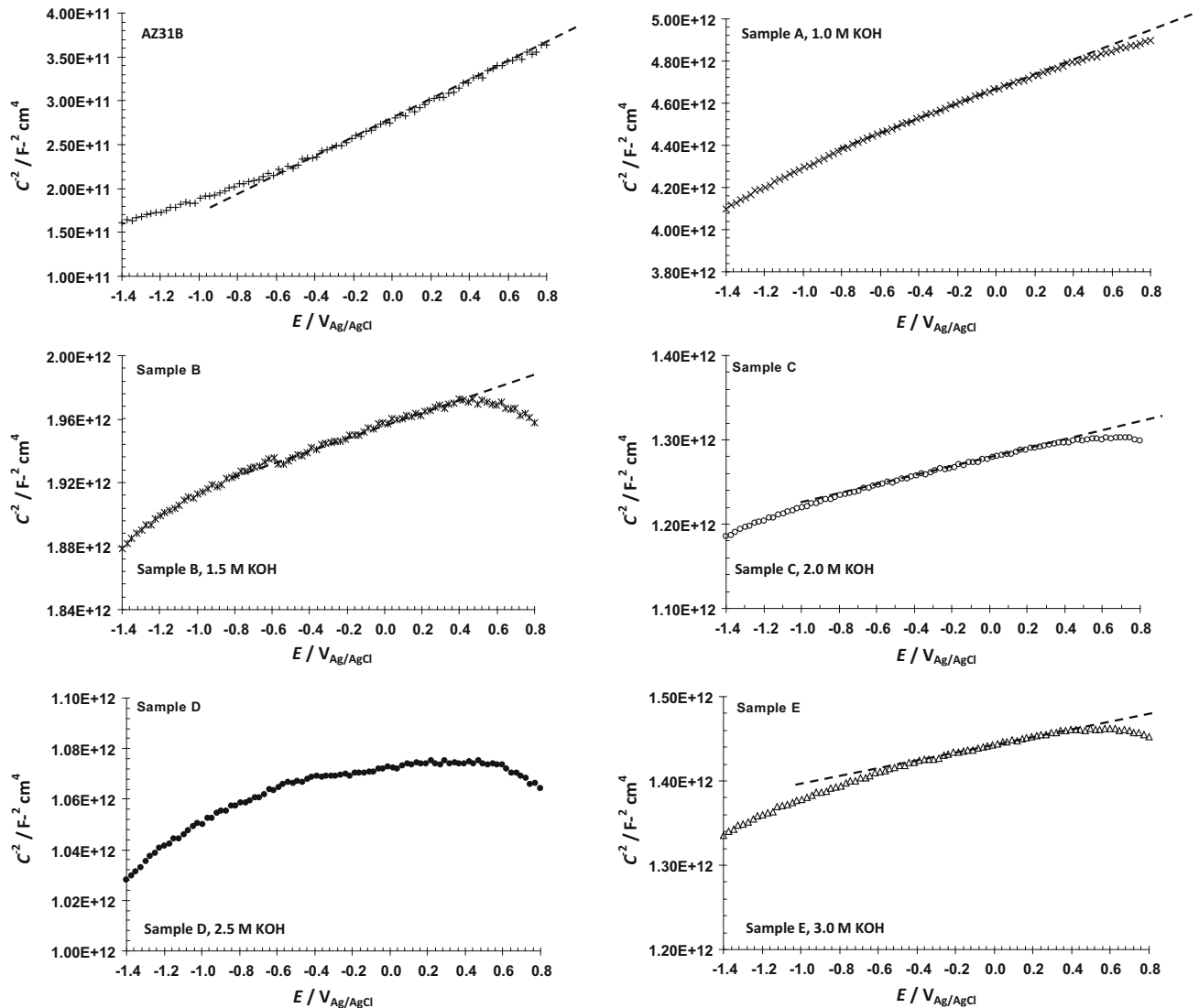


Fig. 8 Mott-Schottky plots of AZ31B Mg alloy with and without MAO coatings in 0.01 M NaOH solution

3.5 EIS Measurements

EIS was used to study the corrosion behavior of the MAO-coated specimens and the uncoated AZ31 Mg alloy. In Fig. 6, the Nyquist curves obtained from EIS of AZ31B Mg alloy with and without MAO coatings in 0.01 M NaOH solution are shown. Concerning the Nyquist curve for uncoated AZ31 Mg alloy, the equivalent circuit of Fig. 7(a) has been used for findings the best fitness (Ref 74, 75). In this equivalent circuit,

R_s ($\approx 260\ \Omega$) is the solution resistance, and R_{ct} is the resistance of the barrier layer interface in parallel with Q_{dl} . As can be seen in Fig. 6, Nyquist curves for coated samples have similar behaviors. For coated samples, an appropriate equivalent circuit shown in Fig. 7(b) has been used. This equivalent electrical circuit is based on the EIS studies of Gu et al. (Ref 42), Ghasemi et al. (Ref 53), Bala Srinivasan et al. (Ref 55), and Ko et al. (Ref 66) on MAO coatings for Mg alloys. In this

Table 4 Donor density (N_D) values of AZ31B Mg alloy with and without MAO coatings in 0.01 M NaOH solution

	AZ31B	Sample A	Sample B	Sample C	Sample D	Sample E
N_D (cm ⁻³)	2.3×10^{20}	1.6×10^{19}	5.4×10^{18}	3.2×10^{18}	4.5×10^{17}	3.2×10^{18}

equivalent model, R_s is the solution resistance, R_p is the resistance of the porous regions of the MAO coating which is in parallel with Q_B , and R_{ct} is the resistance of the inner barrier layer interface in parallel with Q_{dl} . The corresponding EIS data are shown in Table 3. It can be seen that the value of CPE- C_p is lower than CPE- C_{dl} because the coating is relatively thick compared to the interface layer between the dense layer and the AZ31B Mg alloy substrate.

The impedance of all the coated samples is much higher than the AZ31B Mg alloy. This shows that the MAO is an effective coating process which improves the corrosion resistance of AZ31B Mg alloy. It can be seen that the charge transfer resistance R_{ct} of the MAO coatings are much higher than the corresponding value of R_p . This suggests that the inner dense layer plays a key role in protecting the AZ31B Mg alloy from corrosion (Ref 42). The charge transfer resistance R_{ct} is the dominating parameter for the electrochemical behavior of the coated samples. A sample with a higher R_{ct} value is more corrosion resistant. It can be seen that all coated samples have shown much higher R_{ct} value compared to those of uncoated AZ31B Mg alloy.

3.6 Mott-Schottky Analysis

Generally, more detailed evidences regarding the nature of passive films have been obtained using Mott-Schottky analysis. Figure 8 shows the Mott-Schottky plots of AZ31B Mg alloy with and without MAO coatings in 0.01 M NaOH solution. In all plots, there is a region in which C^{-2} and E possess a somehow linear relationship. The positive slope in this region is attributed to n-type behavior. These observations are agreement with the results obtained in previous works for Mg and its alloys (Ref 74-76). According to Eq 1, donor density has been determined from these positive slopes (Ref 74-76):

$$\frac{1}{C^2} = -\frac{2}{\epsilon\epsilon_0eN_D} \left(E - E_{FB} - \frac{kT}{e} \right) \text{ for n-type semiconductor,} \quad (\text{Eq 1})$$

where e is the electron charge, N_D represents the donor density for n-type semiconductor (cm⁻³), ϵ stands for the dielectric constant of the passive film (usually taken as 9.6 for Mg alloys (Ref 74-76), ϵ_0 denotes the vacuum permittivity, and k , T , and E_{FB} are the Boltzmann constant, absolute temperature, and flat band potential, respectively.

The changes in the donor density correspond to the non-stoichiometry defects in the passive films (Ref 74-77). Based on the point defect model (Ref 78, 79), the cation vacancies are electron acceptors, thereby doping the barrier layer p-type, whereas the oxygen vacancies and the metal interstitials are electron donors, resulting in the n-type doping. In this concept, the dominant point defects in the passive film are considered to be oxygen vacancies and/or cation interstitials acting as electron donors (Ref 72-79).

Table 4 shows the calculated donor density of AZ31B Mg alloy with and without MAO coatings in 0.01 M NaOH solution. The orders of donor density magnitude are compa-

table to those reported in other studies (Ref 42, 74, 75). As for samples with different MAO coatings, although the phase constituents and chemical composition of the MAO coatings were not similar, the MAO coatings had similar semiconducting behavior but with the different donor density.

It can be observed that the donor density of AZ31D Mg alloy was much higher than those of the samples with MAO coatings. Also, it is observed that the donor density of the samples with MAO coatings decreases with increasing the KOH concentration up to 2.5 M, while it increases when the KOH concentration reaches 3.0 M. This can be correlated with the different interfacial reactivity of these samples with or without MAO coatings during immersion in 0.01 M NaOH solution. As to the AZ31D Mg alloy, the semiconducting behavior represented the reaction characteristic of a nature passive film formed on this alloy (Ref 74, 75), while the semiconducting behavior of samples with MAO coatings reflected the reaction characteristics of the Mg electrode with MAO coatings during immersion. The higher donor density of the AZ31D Mg alloy than those of samples with MAO coatings was resulted from the higher reactivity of the substrate for the weak protectiveness of the nature passive film.

It is concluded that the Mott-Schottky analysis (capacitance measurement) showed similar results with that of potentiodynamic polarization and EIS measurements and the corrosion results obtained from the DC electrochemical techniques are qualitatively correlated to the donor concentration of the films obtained by Mott-Schottky analysis. Therefore, Mott-Schottky analysis may be regarded as a useful technique for the assessment of quality of MAO coatings formed on Mg alloys.

4. Conclusion

Effect of electrolyte chemistry (KOH concentration) on the morphological, structural, and electrochemical properties of MAO coatings formed on AZ31B Mg alloy was studied in the present work. Conclusions drawn from the study are as follows:

1. Microstructure observations showed that with increasing KOH concentration from 1.0 to 2.5 M, the average pore size and porosity percentage decrease. However, increasing the concentration of 2.5 to 3.0 M causes a deleterious effect on the obtained coating porosity.
2. XRD patterns revealed that anions from the $\text{Na}_3\text{PO}_4 \cdot 10\text{H}_2\text{O}$ and $\text{Na}_2\text{B}_4\text{O}_7 \cdot 5\text{H}_2\text{O}$ additives contributed to react with Mg^{2+} from substrate dissolution and formed the compounds in the coating such as $\text{Mg}_3(\text{PO}_4)_2$ and $\text{Mg}_2\text{B}_2\text{O}_5$.
3. Potentiodynamic polarization plots, EIS measurements, and Mott-Schottky analysis showed that MAO process can significantly improve the electrochemical behavior of AZ31B Mg alloy.
4. Mott-Schottky analysis indicated that the semiconducting characteristic of AZ31B Mg alloy with and without

MAO coatings displayed the n-type behavior, where the oxygen vacancies and interstitials (over the metal vacancies) preponderated.

5. Among the MAO-treated samples, the sample D, electrolyte solution containing 2.5 M KOH, exhibited the least corrosion current density and the lowest donor density, which resulted in its high corrosion resistance compared to that of the untreated substrate and other MAO-treated samples.

References

1. M. Liu, P.J. Uggowizer, A.V. Nagasekhar, P. Schmutz, M. Easton, G.-L. Song, and A. Atrens, Calculated Phase Diagrams and the Corrosion of Die-Cast Mg–Al Alloys, *Corros. Sci.*, 2009, **51**, p 602–619
2. M. Pourbaix, *Atlas of Electrochemical Equilibria in Aqueous Solutions*, 2nd ed., NACE, Houston, 1974
3. W.A. Ferrando, Review of Corrosion and Corrosion Control of Magnesium Alloys and Composites, *J. Mater. Eng.*, 1989, **11**, p 299–313
4. A.S. Hamdy and D.P. Butt, Corrosion Mitigation of Rare-Earth Metals Containing Magnesium EV31A-T6 Alloy via Chrome-Free Conversion Coating Treatment, *Electrochim. Acta*, 2013, **108**, p 852–859
5. R.-C. Zeng, F. Zhang, Z.-D. Lan, H.-Z. Cui, and E.-H. Han, Corrosion Resistance of Calcium-Modified Zinc Phosphate Conversion Coatings on Magnesium–Aluminium Alloys, *Corros. Sci.*, 2014, **88**, p 452–459
6. H.H. Elsentriecy, J. Qu, H. Luo, H.M. Meyer, C. Ma, and M. Chi, Improving Corrosion Resistance of AZ31B Magnesium Alloy via a Conversion Coating Produced by a Protic Ammonium-Phosphate Ionic Liquid, *Thin Solid Films*, 2014, **568**, p 44–51
7. S. Mu, J. Du, H. Jiang, and W. Li, Composition Analysis and Corrosion Performance of a Mo–Ce Conversion Coating on AZ91 Magnesium Alloy, *Surf. Coat. Technol.*, 2014, **254**, p 364–370
8. Q. Zong, L. Wang, W. Sun, and G. Liu, Active Deposition of Bis(8-hydroxyquinoline) Magnesium Coating for Enhanced Corrosion Resistance of AZ91D Alloy, *Corros. Sci.*, 2014, **89**, p 127–136
9. H.R. Bakhsheshi-Rad, E. Hamzah, M. Daroonparvar, S.N. Saud, and M.R. Abdul-kadir, Bi-layer Nano-TiO₂/FHA Composite Coatings on Mg–Zn–Ce Alloy Prepared by Combined Physical Vapour Deposition and Electrochemical Deposition Methods, *Vacuum*, 2014, **110**, p 127–135
10. M. Daroonparvar, M.A.M. Yajid, N.M. Yusof, H.R. Bakhsheshi-Rad, E. Hamzah, and H.A. Kamali, Microstructural Characterization and Corrosion Resistance Evaluation of Nanostructured Al and Al/AlCr Coated Mg–Zn–Ce–La Alloy, *J. Alloys Compd.*, 2014, **615**, p 657–671
11. J. Xu, B. Zou, X. Fan, S. Zhao, Y. Hui, Y. Wang, X. Zhou, X. Cai, S. Tao, H. Ma, and X. Cao, Reactive Plasma Spraying Synthesis and Characterization of TiB₂–TiC–Al₂O₃/Al Composite Coatings on a Magnesium Alloy, *J. Alloys Compd.*, 2014, **596**, p 10–18
12. D. Thirumalaikumarasamy, K. Shanmugam, and V. Balasubramanian, Corrosion Performance of Atmospheric Plasma Sprayed Alumina Coatings on AZ31B Magnesium Alloy Under Immersion Environment, *J. Asian Ceram. Soc.*, 2014, **2**, p 403–415
13. X. Fan, B. Zou, L. Gu, C. Wang, Y. Wang, W. Huang, L. Zhu, and X. Cao, Investigation of the Bond Coats for Thermal Barrier Coatings on Mg Alloy, *Appl. Surf. Sci.*, 2013, **265**, p 264–273
14. C. Xu, L. Chen, L. Yu, J. Zhang, Z. Zhang, and J. Wang, Effect of Pickling Processes on the Microstructure and Properties of Electroless Ni–P Coating on Mg–7.5 Li–2Zn–1Y Alloy, *Prog. Nat. Sci.*, 2014, **24**, p 655–662
15. X. Guo, S. Wang, J. Gong, J. Guo, L. Peng, and W. Ding, Characterization of Highly Corrosion-Resistant Nanocrystalline Ni Coating Electrodeposited on Mg–Nd–Zn–Zr Alloy from a Eutectic-Based Ionic Liquid, *Appl. Surf. Sci.*, 2014, **313**, p 711–719
16. J. Zhang and Z. Kang, Effect of Different Liquid–Solid Contact Models on the Corrosion Resistance of Superhydrophobic Magnesium Surfaces, *Corros. Sci.*, 2014, **87**, p 452–459
17. S.R. Paital, A. Bhattacharya, M. Moncayo, Y.H. Ho, K. Mahdak, S. Nag, R. Banerjee, and N.B. Dahotre, Improved Corrosion and Wear Resistance of Mg Alloys via Laser Surface Modification of Al on AZ31B, *Surf. Coat. Technol.*, 2012, **206**, p 2308–2315
18. J. Dutta Majumdar and I. Manna, Laser Treatment to Improve the Corrosion Resistance of Magnesium (Mg) Alloys, *Corrosion Prevention of Magnesium Alloys*, G.-L. Song, Ed., Woodhead Publishing, Cambridge, 2013,
19. X.-J. Cui, X.-Z. Lin, C.-H. Liu, R.-S. Yang, X.-W. Zheng, and M. Gong, Fabrication and Corrosion Resistance of a Hydrophobic Micro-arc Oxidation Coating on AZ31Mg Alloy, *Corros. Sci.*, 2015, **90**, p 402–412
20. Z. Jia, M. Li, Q. Liu, X. Xu, Y. Cheng, Y. Zheng, T. Xi, and S. Wei, Micro-arc Oxidization of a Novel Mg–Ca Alloy in Three Alkaline KF Electrolytes: Corrosion Resistance and Cytotoxicity, *Appl. Surf. Sci.*, 2014, **292**, p 1030–1039
21. Y. Li, F. Lu, H. Li, W. Zhu, H. Pan, G. Tan, Y. Lao, C. Ning, and G. Ni, Corrosion Mechanism of Micro-arc Oxidation Treated Biocompatible AZ31 Magnesium Alloy in Simulated Body Fluid, *Prog. Nat. Sci.*, 2014, **24**, p 516–522
22. D. Veys-Renaux, C.-E. Barchiche, and E. Rocca, Corrosion Behavior of AZ91Mg Alloy Anodized by Low-Energy Micro-arc Oxidation: Effect of Aluminates and Silicates, *Surf. Coat. Technol.*, 2014, **251**, p 232–238
23. Z. Song, Z. Xie, G. Yu, B. Hu, X. He, and X. Zhang, A Novel Palladium-Free Surface Activation Process for Electroless Nickel Deposition on Micro-arc Oxidation Film of AZ91D Mg Alloy, *J. Alloys Compd.*, 2015, **623**, p 274–281
24. C. Wang, B. Jiang, M. Liu, and Y. Ge, Corrosion Characterization of Micro-arc Oxidization Composite Electrophoretic Coating on AZ31B Magnesium Alloy, *J. Alloys Compd.*, 2015, **621**, p 53–61
25. D. Veys-Renaux, E. Rocca, J. Martin, and G. Henrion, Initial stages of AZ91Mg Alloy Micro-arc Anodizing: Growth Mechanisms and Effect on the Corrosion Resistance, *Electrochim. Acta*, 2014, **124**, p 36–45
26. Y. Xiong, C. Lu, C. Wang, and R. Song, The n-MAO/EPD Bio-ceramic Composite Coating Fabricated on ZK60 Magnesium Alloy Using Combined Micro-arc Oxidation with Electrophoretic Deposition, *Appl. Surf. Sci.*, 2014, **322**, p 230–235
27. R. Zhang, Y. Zhang, S. Zhang, B. Qu, S. Guo, and J. Xiang, Formation Process of Micro Arc Oxidation Coatings Obtained in a Sodium Phytate Containing Solution With and Without CaCO₃ on Binary Mg–1.0 Ca Alloy, *Appl. Surf. Sci.*, 2015, **325**, p 79–85
28. M. Li, J. Liu, J. Li, Y. Li, S. Lu, and Y. Yuan, The Enhanced Corrosion Resistance of UMAO Coatings on Mg by Silane Treatment, *Prog. Nat. Sci.*, 2014, **24**, p 486–491
29. Y. Ge, B. Jiang, M. Liu, C. Wang, and W. Shen, Preparation and Characterization of the Micro-arc Oxidation Composite Coatings on Magnesium Alloys, *J. Magnes. Alloys*, 2014, **2**, p 309–316
30. L.-H. Li, T.S. Narayanan, Y.K. Kim, Y.-M. Kong, I.S. Park, T.S. Bae, and M.H. Lee, Deposition of Microarc Oxidation–Polycaprolactone Duplex Coating to Improve the Corrosion Resistance of Magnesium for Biodegradable Implants, *Thin Solid Films*, 2014, **562**, p 561–567
31. B. Salami, A. Afshar, and A. Mazaheri, The Effect of Sodium Silicate Concentration on Microstructure and Corrosion Properties of MAO-Coated Magnesium Alloy AZ31 in Simulated Body Fluid, *J. Magnes. Alloys*, 2014, **2**, p 72–77
32. X. Ma, S. Zhu, L. Wang, C. Ji, C. Ren, and S. Guan, Synthesis and Properties of a Bio-composite Coating Formed on Magnesium Alloy by One-Step Method of Micro-arc Oxidation, *J. Alloys Compd.*, 2014, **590**, p 247–253
33. Y. Xiong, C. Lu, C. Wang, and R. Song, Degradation Behavior of n-MAO/EPD Bio-ceramic Composite Coatings on Magnesium Alloy in Simulated Body Fluid, *J. Alloys Compd.*, 2015, **625**, p 258–265
34. G. Cao, L. Wang, Z. Fu, J. Hu, S. Guan, C. Zhang, L. Wang, and S. Zhu, Chemically Anchoring of TiO₂ Coating on OH-Terminated Mg₃(PO₃)₂ Surface and Its Influence on the In Vitro Degradation Resistance of Mg–Zn–Ca Alloy, *Appl. Surf. Sci.*, 2014, **308**, p 38–42
35. M. Razavi, M. Fathi, O. Savabi, B.H. Beni, D. Vashaee, and L. Tayebi, Nanostructured Merwinite Bioceramic Coating on Mg Alloy Deposited by Electrophoretic Deposition, *Ceram. Int.*, 2014, **40**, p 9473–9484
36. Y. Pan, C. Chen, D. Wang, and D. Huang, Dissolution and Precipitation Behaviors of Silicon-Containing Ceramic Coating on Mg–Zn–Ca Alloy in Simulated Body Fluid, *Colloids Surf. B*, 2014, **122**, p 746–751
37. Y. Lu, P. Wan, L. Tan, B. Zhang, K. Yang, and J. Lin, Preliminary Study on a Bioactive Sr Containing Ca–P Coating on Pure Magnesium by a Two-Step Procedure, *Surf. Coat. Technol.*, 2014, **252**, p 79–86

38. M. Razavi, M. Fathi, O. Savabi, D. Vashae, and L. Tayebi, In Vitro Study of Nanostructured Diopside Coating on Mg Alloy Orthopedic Implants, *Mater. Sci. Eng. C*, 2014, **41**, p 168–177
39. M. Razavi, M. Fathi, O. Savabi, B. Hashemibeni, D. Vashae, and L. Tayebi, Surface Microstructure and In Vitro Analysis of Nanostructured Akermanite ($\text{Ca}_2\text{MgSi}_2\text{O}_7$) Coating on Biodegradable Magnesium Alloy for Biomedical Applications, *Colloids Surf. B*, 2014, **117**, p 432–440
40. M. Razavi, M. Fathi, O. Savabi, S.M. Razavi, F. Heidari, M. Manshaei, D. Vashae, and L. Tayebi, In Vivo Study of Nanostructured Diopside ($\text{CaMgSi}_2\text{O}_6$) Coating on Magnesium Alloy as Biodegradable Orthopedic Implants, *Appl. Surf. Sci.*, 2014, **313**, p 60–66
41. S.-D. Wu, H. Zhang, X.-D. Dong, C.-Y. Ning, A.S.L. Fok, and Y. Wang, Physicochemical Properties and In Vitro Cytocompatibility of Modified Titanium Surfaces Prepared via Micro-arc Oxidation with Different Calcium Concentrations, *Appl. Surf. Sci.*, 2015, **329**, p 347–355
42. Y. Gu, C.-F. Chen, S. Bandopadhyay, C. Ning, Y. Zhang, and Y. Guo, Corrosion Mechanism and Model of Pulsed DC Microarc Oxidation Treated AZ31 Alloy in Simulated Body Fluid, *Appl. Surf. Sci.*, 2012, **258**, p 6116–6126
43. D. Wu, X. Liu, K. Lu, Y. Zhang, and H. Wang, Influence of $\text{C}_3\text{H}_8\text{O}_3$ in the Electrolyte on Characteristics and Corrosion Resistance of the Microarc Oxidation Coatings Formed on AZ91D Magnesium Alloy Surface, *Appl. Surf. Sci.*, 2009, **255**, p 7115–7120
44. S. Xin, L. Song, R. Zhao, and X. Hu, Influence of Cathodic Current on Composition, Structure and Properties of Al_2O_3 Coatings on Aluminum Alloy Prepared by Micro-arc Oxidation Process, *Thin Solid Films*, 2006, **515**, p 326–332
45. J. Liang, L. Hu, and J. Hao, Improvement of Corrosion Properties of Microarc Oxidation Coating on Magnesium Alloy by Optimizing Current Density Parameters, *Appl. Surf. Sci.*, 2007, **253**, p 6939–6945
46. L. Wang, J. Zhou, J. Liang, and J. Chen, Microstructure and Corrosion Behavior of Plasma Electrolytic Oxidation Coated Magnesium Alloy Pretreated by Laser Surface Melting, *Surf. Coat. Technol.*, 2012, **206**, p 3109–3115
47. R.F. Zhang, Film Formation in the Second Step of Micro-arc Oxidation on Magnesium Alloys, *Corros. Sci.*, 2010, **52**, p 1285–1290
48. H.F. Guo, M.Z. An, H.B. Huo, S. Xu, and L.J. Wu, Microstructure Characteristic of Ceramic Coatings Fabricated on Magnesium Alloys by Micro-arc Oxidation in Alkaline Silicate Solutions, *Appl. Surf. Sci.*, 2006, **252**, p 7911–7916
49. J. Cai, F. Cao, L. Chang, J. Zheng, J. Zhang, and C. Cao, The Preparation and Corrosion Behaviors of MAO Coating on AZ91D with Rare Earth Conversion Precursor Film, *Appl. Surf. Sci.*, 2011, **257**, p 3804–3811
50. J. Liang, B. Guo, J. Tian, H. Liu, J. Zhou, and T. Xu, Effect of Potassium Fluoride in Electrolytic Solution on the Structure and Properties of Microarc Oxidation Coatings on Magnesium Alloy, *Appl. Surf. Sci.*, 2005, **252**, p 345–351
51. H. Luo, Q. Cai, B. Wei, B. Yu, D. Li, J. He, and Z. Liu, Effect of $(\text{NaPO}_3)_6$ Concentrations on Corrosion Resistance of Plasma Electrolytic Oxidation Coatings Formed on AZ91D Magnesium Alloy, *J. Alloys Compd.*, 2008, **464**, p 537–543
52. L. Shi, Y. Xu, K. Li, Z. Yao, and S. Wu, Effect of Additives on Structure and Corrosion Resistance of Ceramic Coatings on Mg–Li Alloy by Micro-arc Oxidation, *Curr. Appl. Phys.*, 2010, **10**, p 719–723
53. A. Ghasemi, V.S. Raja, C. Blawert, W. Dietzel, and K.U. Kainer, The Role of Anions in the Formation and Corrosion Resistance of the Plasma Electrolytic Oxidation Coatings, *Surf. Coat. Technol.*, 2010, **204**, p 1469–1478
54. S. Durdu and M. Usta, Characterization and Mechanical Properties of Coatings on Magnesium by Micro Arc Oxidation, *Appl. Surf. Sci.*, 2012, **261**, p 774–782
55. P. Bala Srinivasan, J. Liang, R.G. Balajee, C. Blawert, M. Störmer, and W. Dietzel, Effect of Pulse Frequency on the Microstructure, Phase Composition and Corrosion Performance of a Phosphate-Based Plasma Electrolytic Oxidation Coated AM50 Magnesium Alloy, *Appl. Surf. Sci.*, 2010, **256**, p 3928–3935
56. Q. Wen, F.H. Cao, Y.Y. Shi, Z. Zhang, and J.Q. Zhang, The Effect of Phosphate on MAO of AZ91D Magnesium Using AC Power Source, *Mater. Corros.*, 2008, **59**, p 819–824
57. R.F. Zhang, S.F. Zhang, Y.L. Shen, L.H. Zhang, T.Z. Liu, Y.Q. Zhang, and S.B. Guo, Influence of Sodium Borate Concentration on Properties of Anodic Coatings Obtained by Micro Arc Oxidation on Magnesium Alloys, *Appl. Surf. Sci.*, 2012, **258**, p 6602–6610
58. C.S. Wu, Z. Zhang, F.H. Cao, L.J. Zhang, J.Q. Zhang, and C.N. Cao, Study on the Anodizing of AZ31 Magnesium Alloys in Alkaline Borate Solutions, *Appl. Surf. Sci.*, 2007, **253**, p 3893–3898
59. A. Bai and Z.-J. Chen, Effect of Electrolyte Additives on Anti-corrosion Ability of Micro-arc Oxide Coatings Formed on Magnesium Alloy AZ91D, *Surf. Coat. Technol.*, 2009, **203**, p 1956–1963
60. A. Da Forno and M. Bestetti, Effect of the electrolytic solution Composition on the Performance of Micro-arc Anodic Oxidation Films Formed on AM60B Magnesium Alloy, *Surf. Coat. Technol.*, 2010, **205**, p 1783–1788
61. C.E. Barchiche, E. Rocca, and J. Hazan, Corrosion Behaviour of Sn-Containing Oxide Layer on AZ91D Alloy Formed by Plasma Electrolytic Oxidation, *Surf. Coat. Technol.*, 2008, **202**, p 4145–4152
62. C.E. Barchiche, E. Rocca, C. Juers, J. Hazan, and J. Steinmetz, Corrosion Resistance of Plasma-Anodized AZ91D Magnesium Alloy by Electrochemical Methods, *Electrochim. Acta*, 2007, **53**, p 417–425
63. F.H. Cao, J.L. Cao, Z. Zhang, J.Q. Zhang, and C.N. Cao, Plasma Electrolytic Oxidation of AZ91D Magnesium Alloy with Different Additives and Its Corrosion Behavior, *Mater. Corros.*, 2007, **58**, p 696–703
64. S. Verdier, M. Boinet, S. Maximovitch, and F. Dalard, Formation, Structure and Composition of Anodic Films on AM60 Magnesium Alloy Obtained by DC Plasma Anodizing, *Corros. Sci.*, 2005, **47**, p 1429–1444
65. Y.-L. Cheng, T.W. Qin, L.-L. Li, H.-M. Wang, and Z. Zhang, Comparison of Corrosion Resistance of Microarc Oxidation Coatings Prepared with Different Electrolyte Concentrations on AM60 Magnesium Alloy, *Corros. Eng. Sci. Technol.*, 2011, **46**, p 17–23
66. Y.G. Ko, S. Namgung, and D.H. Shin, Correlation Between KOH Concentration and Surface Properties of AZ91 Magnesium Alloy Coated by Plasma Electrolytic Oxidation, *Surf. Coat. Technol.*, 2010, **205**, p 2525–2531
67. H.F. Guo and M.Z. An, Growth of Ceramic Coatings on AZ91D Magnesium Alloys by Micro-arc Oxidation in Aluminate-Fluoride Solutions and Evaluation of Corrosion Resistance, *Appl. Surf. Sci.*, 2005, **246**, p 229–238
68. H. Duan, K. Du, C. Yan, and F. Wang, Electrochemical Corrosion Behavior of Composite Coatings of Sealed MAO Film on Magnesium Alloy AZ91D, *Electrochim. Acta*, 2006, **51**, p 2898–2908
69. X.G. Han, X.P. Zhu, and M.K. Lei, Electrochemical Properties of Microarc Oxidation Films on a Magnesium Alloy Modified by High-Intensity Pulsed Ion Beam, *Surf. Coat. Technol.*, 2011, **206**, p 874–878
70. W. Mu and Y. Han, Characterization and Properties of the $\text{MgF}_2/\text{ZrO}_2$ Composite Coatings on Magnesium Prepared by Micro-arc Oxidation, *Surf. Coat. Technol.*, 2008, **202**, p 4278–4284
71. W. Xue, Z. Deng, R. Chen, and T. Zhang, Growth Regularity of Ceramic Coatings Formed by Microarc Oxidation on Al–Cu–Mg Alloy, *Thin Solid Films*, 2000, **372**, p 114–117
72. A. Fattah-alhosseini and O. Imantalab, Effect of Accumulative Roll Bonding Process on the Electrochemical Behavior of Pure Copper, *J. Alloys Compd.*, 2015, **632**, p 48–52
73. O. Imantalab and A. Fattah-alhosseini, Electrochemical and Passive Behaviors of Pure Copper Fabricated by Accumulative Roll-Bonding (ARB) Process, *JMEPEG*, 2015, **24**, p 2579–2585
74. A. Fattah-alhosseini and M. Sabaghi Joni, Role of Chloride in the Electrochemical Behaviour of AZ31B Mg Alloy, *Int. J. Mater. Res.*, 2015, **106**, p 282–287
75. A. Fattah-alhosseini and M. Sabaghi Joni, Effect of Immersion Time on the Electrochemical Behaviour of AZ31B Alloy, *J. Alloys Compd.*, 2015, **646**, p 685–691
76. H. Duan, C. Yan, and F. Wang, Effect of Electrolyte Additives on Performance of Plasma Electrolytic Oxidation Films Formed on Magnesium Alloy AZ91D, *Electrochim. Acta*, 2007, **52**, p 3785–3793
77. K. Venkateswarlu, N. Rameshbabu, D. Sreekanth, M. Sandhyarani, A.C. Bose, V. Muthupandi, and S. Subramanian, Role of Electrolyte Chemistry on Electronic and In Vitro Electrochemical Properties of Micro-arc Oxidized Titania Films on Cp Ti, *Electrochim. Acta*, 2013, **105**, p 468–480
78. D.D. Macdonald, On the Existence of Our Metals-Based Civilization I. Phase-Space Analysis, *J. Electrochem. Soc.*, 2006, **153**, p B213–B224
79. D.D. Macdonald, On the Tenuous Nature of Passivity and Its Role in the Isolation of HLNW, *J. Nucl. Mater.*, 2008, **379**, p 24–32